



Internal variability in multidecadal trends of surface air temperature over antarctica in austral winter in model simulations

Ya Wang^{1,3} · Gang Huang^{1,2,3} · Kaiming Hu¹

Received: 29 October 2019 / Accepted: 7 August 2020 / Published online: 12 August 2020
© Springer-Verlag GmbH Germany, part of Springer Nature 2020

Abstract

The surface air temperature (SAT) exhibits pronounced warming over West Antarctica in recent decades, especially in austral spring and winter. Using a 30-member ensemble of simulations by Community Earth System Model (CESM), two reanalysis datasets, and observed station data, this study investigates the relative contributions of internally generated low-frequency climate variability and externally forced climate change to the austral winter SAT trend in Antarctica. Although these simulations share the same external forcing, the SAT trends during 1979–2005 show large diversity among the individual members in the CESM ensemble simulations, suggesting that internally generated variability contributes a considerable part to the multidecadal SAT change in Antarctica. Quantitatively, the total forced contribution to the SAT (1979–2005) change is about 0.53 k/27 yr, and the internal variability can be strong enough to double or cancel the externally forced warming trend. A method called “dynamical adjustment” is utilized to further divide the forced response. We find both the forced thermodynamically-induced and the forced dynamically-induced SAT trends are positive over all the regions in Antarctica, with the regional mean values of 0.20 k/27 yr and 0.33 k/27 yr, respectively. The diversity of SAT trends among the simulations is closely linked to a Southern hemisphere Annular Mode (SAM)-like atmospheric circulation multidecadal change in the Southern Hemisphere. When there exists a positive–negative seesaw of pressure trend between Antarctica and the mid-latitudes, the SAT trend is positive over most of Antarctica but negative over the Antarctic Peninsula, and vice versa. The SAM-like atmospheric circulation multidecadal change mainly arises from atmospheric internal variability rather than remote tropical Sea Surface Temperature (SST).

Keywords Internal variability · Antarctica · SAM · CESM · Dynamic adjustment

1 Introduction

Evaluating the uncertainties of climate projections plays an important role in both developing models and making policy decisions for stakeholders and policymakers. There has been substantial progress in the assessment of uncertainties of climate projection in the last decade. Uncertainties in climate model attribute to three different sources (Hawkins and Sutton 2009): model uncertainty, internal variability, and scenario uncertainty Hawkins and Sutton (2011). found that the internal variability and model uncertainty are the dominant sources for the surface air temperature (SAT) in Coupled Model Intercomparison Project3 (CMIP3) simulations. Using large ensemble projections, Deser et al. (2012), Wallace et al. (2012) and Lehner et al. (2020) show that climate system internal variability could be strong enough to double or cancel the upward trend of regional air temperature in response to the build-up of greenhouse gases on

✉ Gang Huang
hg@mail.iap.ac.cn

✉ Kaiming Hu
hkm@mail.iap.ac.cn

¹ State Key Laboratory of Numerical Modeling for Atmospheric Sciences and Geophysical Fluid Dynamics and Center for Monsoon System Research, Institute of Atmospheric Physics, Chinese Academy of Sciences, LASG/IAP/CAS, P.O. Box 9804, Beijing 100029, China

² Laboratory for Regional Oceanography and Numerical Modeling, Qingdao National Laboratory for Marine Science and Technology, Qingdao 266237, China

³ University of Chinese Academy of Sciences, Beijing 100049, China

the multidecadal time scale. Thus, it is important to evaluate the role of internal variability in regional climate change.

Observed evidence shows that the SAT in Antarctica has experienced a significant change in recent decades, which is generally associated with the modulation of atmospheric circulation. More northerly wind anomalies could lead to warm advection, causing a positive SAT trend and vice versa (Raphael et al. 2016). Part of the SAT trend in Antarctica is likely due to human activities. For example, in response to the ozone depletion, the Southern hemisphere Annular Mode (SAM) became stronger during 1979–2000, which in turn led to an increasing trend of SAT over the Peninsula in austral summer (Arblaster and Meehl 2006; Fogt et al. 2009; Ivy et al. 2017; Seviour et al. 2016; Thompson et al. 2011). Meanwhile, internally generated variability can also lead to SAT change on the multidecadal time scale (Ding et al. 2011; Li et al. 2014, 2015; Schneider and Deser 2018; Schneider et al. 2012). For example, rapid warming over West Antarctica in recent decades is likely driven by multidecadal sea surface temperature (SST) variability in the tropical Pacific and North Atlantic via strengthening the Amundsen Sea Low (ASL). However, the relative contributions of internal variability and external forcing to the SAT trend in Antarctica are still unknown.

It is often difficult to distinguish between internally generated low-frequency climate variability and externally forced climate change. There exist two obstacles to this problem: Firstly, only a few methods can be used to discriminate these two parts; Secondly, it is also a big challenge to verify whether the method is effective since the true values of these two parts stay unknown. Large ensembles of the same model sharing the same external forcing could help analyze this problem. As the only difference between these ensembles is the initial condition, the ensemble mean trend can be treated as the externally forced response and the departures of these trends in individual members from the ensemble mean are identified as the internal variability. Deser et al. (2012) have studied the internal variability of the atmosphere in tropical and ex-tropical areas in the southern hemisphere by the Version 3 of the Community Climate System Model (CCSM3) Large Ensemble, and further separated the forced responses to thermodynamical and dynamical contributions (Deser et al. 2016). Hu et al. (2018) used the Version 4 of the Community Climate System Model (CCSM4) data to analyze the leading internal variability of the SAT in East Asia. Here we use the Community Earth System Model (CESM) Large Ensemble (Kay et al. 2015) to further explore this problem over Antarctica.

This study aims to evaluate the internally generated and externally forced multidecadal SAT change over Antarctica in austral winter. We focus on austral winter because wintertime internal variability in SAT multidecadal change is generally larger than that in summer (Deser et al. 2012).

The rest of this study is organized as follows. Section “2” describes the data and methods. Section “3” evaluates the CESM simulations over Antarctica. Section “4” calculates the contribution of external and internal variability to the SAT trends in the simulations. The thermodynamic and dynamic contribution to the SAT trends of the Reanalysis datasets is presented in Sect. “5”. Section “6” presents the leading internal variability of SAT and the related circulations in the CESM simulations. Section “7” presents the summary and discussion.

2 Data and method

We utilize the CESM1 (CAM5) Large Ensemble simulations (Kay et al. 2015) of the historical run (1979–2005) with a horizontal resolution of about $1^\circ \times 1^\circ$. The model is a coupled climate model composed of atmosphere, ocean, land, and sea ice component models. The historical ensemble members undergo the same observationally estimated radiative forcing except for the ozone forcing, following the instruction in phase 5 of the Coupled Model Intercomparison Project (CMIP5) design protocol (Taylor et al. 2012). The ozone concentrations in CESM Large Ensemble are calculated by the Whole Atmosphere Community Climate Model (WACCM) (Marsh et al. 2013), whose result is considered to be more accurate than that used in CMIP5. The only difference between these ensembles is the initial conditions. Specifically, random round-off level differences to the air temperature are used to generate the atmospheric initial conditions. To analyze the internal variability generated only by the atmospheric system, we also use 2600 years of atmosphere-only control run with atmosphere and land components, forced by prescribed yearly repeated monthly mean SST and sea ice. The data are part of the CESM1 Large Ensemble (Kay et al. 2015), which could be download from the NCAR archive. In addition to the above data, the monthly outputs from 42 CMIP5 models of the historical simulations are also used and interpolated into $2.5^\circ \times 2.5^\circ$ horizontal resolution. The models and detailed information are listed in Table 1 (Taylor et al. 2012). To compare with the simulations, the Merra Reanalysis (Rienecker et al. 2011), ERA-Interim (Berrisford et al. 2011) are added. The READER station data (Turner et al. 2004) during 1979–2005 is adopted as observed data and is archived by the British Antarctic Survey.

The term “trend” throughout this article is calculated by the linear least-squares fitting to the period 1979–2005. To further explore the relationship between circulation and SAT, a singular value decomposition (SVD) method is used to examine the linkage between the austral wintertime Antarctic SAT trends and the simultaneous southern hemisphere sea level pressure (SLP) trends. We also use an empirical

Table 1 List of 42 CMIP5 models used in this study

Model	Institution
ACCESS1.0 ACCESS1.3	Commonwealth scientific and industrial research organization (CSIRO) and the bureau of meteorology, Australia
BCC_CSM1.1(M) BCC-CSM1.1	Beijing climate center, China meteorological administration, China
BNU-ESM	College of global change and earth system science, Beijing normal university, China
CANCM4 CANESM2	Canadian centre for climate modeling and analysis, Canada
CCSM4	National center for atmospheric research (NCAR), United States
CMCC-CM CMCC-CMS	Centro Euro-Mediterraneo per I Cambiamenti Climatici, Italy
CESM1-BGC CESM1-CAM5 CESM1-FASTCHEM CESM1-WACCM	National science foundation (NSF), U.S. department of energy, and NCAR, United States
CNRM-CM5	Centre national de recherches Météorologiques, France
CSIRO-MK3.6.0	CSIRO in collaboration with the queensland climate change centre of excellence, Australia
FGOALS-G2 FGOALS-S2	LASG, institute of atmospheric physics, chinese academy of sciences, China
FIO-ESM	First institute of oceanography (SOA), China
GFDL-CM2P1 GFDL-CM3 GFDL-ESM2G GFDL-ESM2M	GFDL, United States
GISS-E2-H GISS-E2-R	NASA goddard institute for space studies, United States
HADCM3 HADGEM2-AO HADGEM2-CC HADGEM2-ES	Met office hadley centre, United Kingdom
INM-CM4.0	Russian institute for numerical mathematics, Russia
IPSL-CM5A-LR IPSL-CM5A-MR IPSL-CM5B-LR	IPSL, France
MIROC4h MIROC5 MIROC-ESM-CHEM MIROC-ESM	The university of Tokyo, national institute for environmental studies, and Japan agency for marine-earth science and technology, Japan
MPI-ESM-LR MPI-ESM-MR	Max planck institute for meteorology, Germany
MRI-CGCM3	Meteorological research institute, Japan
NorESM1-ME NorESM1-M	Norwegian climate centre, Norway

orthogonal function (EOF) analysis on the Atmospheric Global Climate Model (AGCM) SAT trends (Kay et al. 2015) of every 27 years to pick up the leading internal variability induced by the atmosphere and land themselves.

Following Wallace et al. (2012), we use a method called “dynamical adjustment” to reduce the internal variability in the winter SAT trend in Antarctica. In this method, the SAT trend related to large scale circulation change is removed based on partial least-square regression. The procedure of this method is described as follows. Firstly, the SLP series is regressed onto the SAT series to generate one-point regression maps in the selected domain calculated grid by grid. Secondly, the SLP series is projected in every member of the ensemble simulations onto the regression map to obtain a weighted series $S(n)$ for every grid of SAT. The weighted series $S(n)$ represents the similarity of regression pattern and SLP series of every year. Thirdly, the array $S(n)$ is regressed out of both the SLP and the SAT series to generate a residual SLP map and SAT sequence for every grid. Here, the residual SAT denotes the SAT without the impact of SLP related to $S(n)$. The above steps are repeated four times using the residual SAT and SLP field to remove the influence of atmospheric

circulation as much as possible. For convenience, the final SAT residual field is hereinafter called the four-pass dynamical adjust SAT trend. In the adjustment, the SAT trend related to large scale atmospheric circulation change is removed, so, the residual SAT trend should be related to the thermodynamic process.

We also use wave-activity fluxes to diagnose the connection between the tropics and Antarctica. The definition of the wave-activity fluxes follows Takaya and Nakamura (2001) as:

$$W = \frac{1}{2|\mathbf{U}|} \begin{pmatrix} \bar{u} (\psi_x'^2 - \psi' \psi_{xx}') + \bar{v} (\psi_x' \psi_y' - \psi' \psi_{xy}') \\ \bar{u} (\psi_x' \psi_y' - \psi' \psi_{xy}') + \bar{v} (\psi_y'^2 - \psi' \psi_{yy}') \\ \frac{f^2}{R\sigma/p} \left\{ \bar{u} (\psi_x' \psi_p' - \psi' \psi_{xp}') + \bar{v} (\psi_y' \psi_p' - \psi' \psi_{yp}') \right\} \end{pmatrix}$$

Here, ψ denotes the stream function, f the Coriolis parameter, R the gas constant, $\mathbf{U} = (u, v)$ the horizontal wind velocity, and $\sigma = (R T / C_p p) - d T / dp$, with temperature T , and the specific heat at constant pressure C_p . Overbars and primes denote the climatology and the anomalies, respectively. The fluxes are parallel to the local group velocity of stationary Rossby wave.

3 Evaluating the CESM simulation over Antarctica

Figure 1a–c show the 1979–2005 climatology of JJA (June–July–August) SAT and SLP over Antarctica in different datasets, the READER station data is added for comparison. For ERA-Interim, the climatological SAT is higher in West Antarctica than in the east. In West Antarctica, climatological SAT ranges from -48 °C to -28 °C, with the maximum temperatures distributed in the Peninsula and Antarctic coast. In East Antarctica, the SAT is lower than -48 °C in most regions. Both the spatial pattern and magnitude of the climatological SAT in ERA-Interim match the observations (READER station data) very well. For Merra data, the climatological SAT is generally comparable with the observed SAT except for East Antarctica, where the SAT is about 5 °C higher than that in the observations. The ensemble-mean climatological SAT in CESM simulations (Fig. 1c) is consistent with the READER data, with lower SAT in East Antarctica. Compared with ERA-Interim, areas with temperatures below -20 °C are more extensive in Merra. For the SLP, three low centers are located around Antarctica in both the reanalysis datasets and the CESM simulations. The simulations basically reproduce the locations and strength of these centers, especially for the one located in the west of the Ross ice shelf, which is also known as the Amundsen Sea Low (ASL).

4 The external and internal variability of SAT trends in the simulations

Figure 2 shows the 1979–2005 JJA SAT trends over Antarctica in the individual members of the CESM ensemble simulations. The epochal differences (1993–2005 minus 1979–1992) are also calculated, a similar result is obtained. Although most members show a warming trend, the diversity among the simulations is quite large. In the west of Antarctica, SAT shows intense warming trends in “C3”, “C5”, “C7”, “C12”, “C28”, but dramatically decreases in “C13” and “C16”. While in the east of Antarctica, warming trends exist in the members “C7”, “C10”, “C12”, and “C19”, but cooling in “C2”, “C9”, “C14”, and “C24”. The large diversity suggests that the simulated multidecadal SAT trends over Antarctica are strongly affected by internal variability. This is consistent with recent work that pointed out the rapid warming in recent decades over the west of Antarctica is likely due to internal variability (Li et al. 2015; Schneider and Deser 2018). For comparison, we calculate 1979–2005 SAT trends in the READER station data as the observed trends. The observed SAT trends show strong warming in the stations over the Antarctic Peninsula and the Indian Ocean sector, but cooling in the Pacific sector, which are similar to the SAT trends in the ensemble members of C15, C25, and C28. The similarity lends some credence to study the internal variability of SAT trends in Antarctica by the large ensemble simulations. In addition, we also compared the observed SAT trends with the trends in the Merra Reanalysis and the ERA-Interim and found that the SAT trends in these two reanalysis datasets have profound difference from the observed, especially in the Antarctic Peninsula.

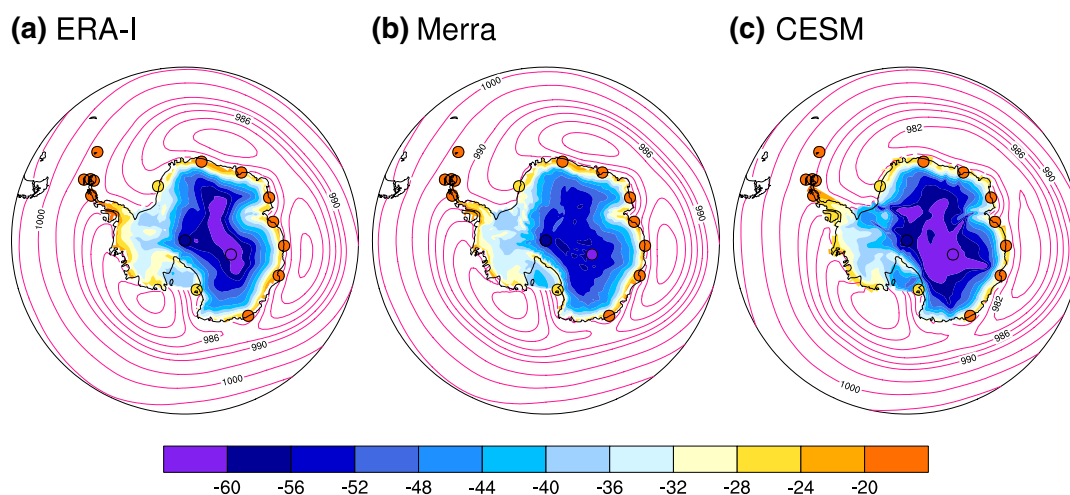


Fig. 1 The climatological JJA SAT (color; °C) and SLP (contour line; hPa) at interval of 2 hPa in ERA-Interim (a), Merra Reanalysis (b), CESM ensemble mean (c), READER station data (circles, with color showing the trends) during 1979–2005

Fig. 2 SAT trends ($^{\circ}\text{C}$; 1979–2005) among the 30 ensembles (labeled c1–c30), Merra Reanalysis (labeled Merra), ERA-Interim (labeled ERA-I), and READER station data (labeled READER)

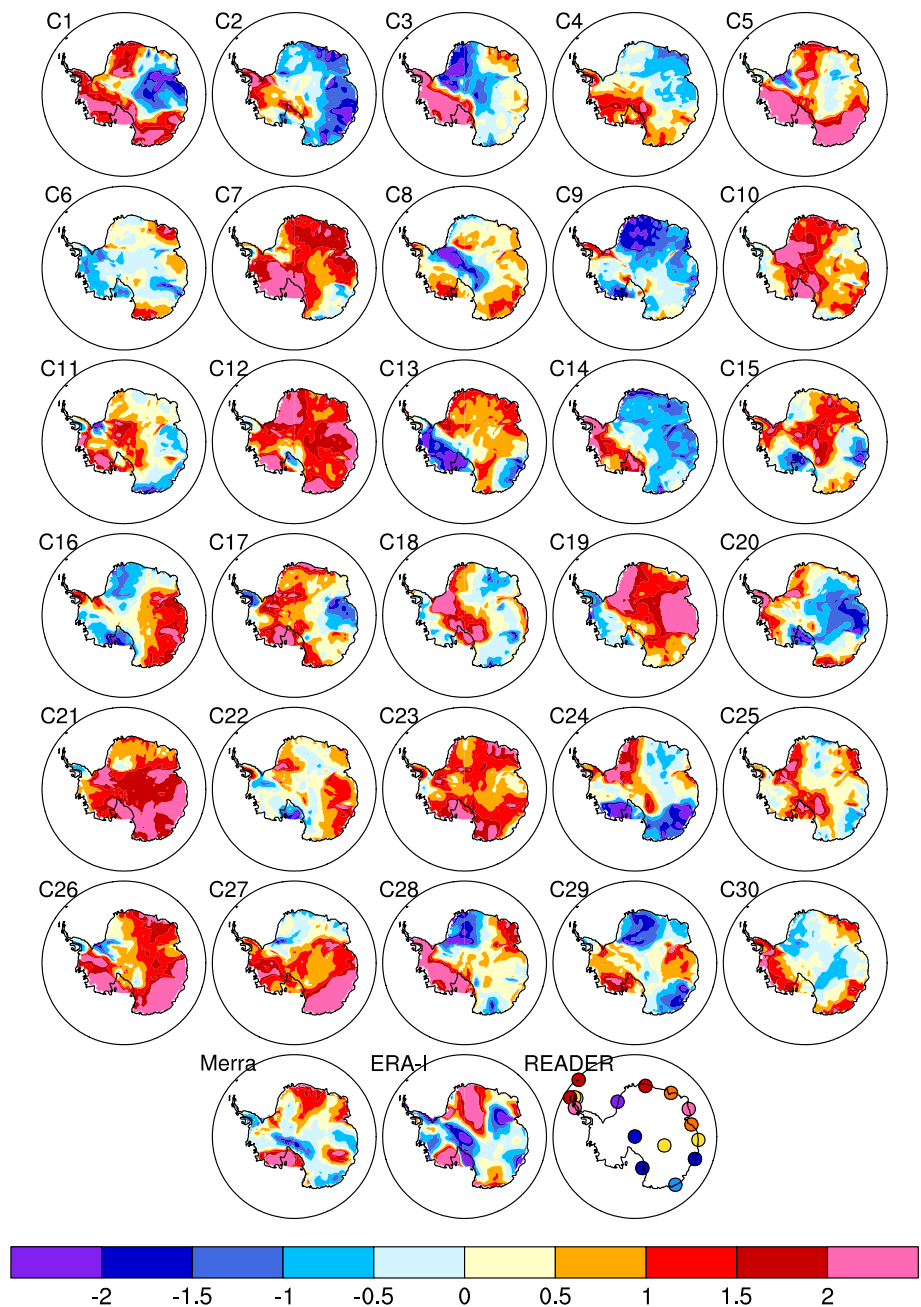


Figure 3a shows the 1979–2005 ensemble-mean SAT trends, which feature increasing temperature over all the Antarctic continent with the maximum warming trend of about $1^{\circ}\text{C}/27\text{ yr}$ around the Ross Ice Shelf area. Associated with the ensemble-mean SAT trends, there is a low-pressure anomaly in the Pacific sector, leading to warm advection over the Ross Ice Shelf. The standard deviations of the SAT trends across the 30 members are lower than $1^{\circ}\text{C}/27\text{ yr}$ in central Antarctica but higher than $2^{\circ}\text{C}/27\text{ yr}$ around the Ross Ice Shelf (Fig. 3b). In order to quantify the relative contribution of internally-generated low-frequency variability and externally forced changes in JJA SAT trends

over Antarctica, we used the signal-to-noise ratio between the ensemble-mean trends and the standard deviation of the departures. The ratio (Fig. 3c) is higher than 1 in central Antarctica, close to or even lower than 1 in West Antarctica and lower than 0.8 around the Antarctic Peninsula, indicating that the wintertime internal variability-induced SAT trends are comparable or even larger than the externally-forced SAT trends in most of Antarctica.

Furthermore, we divide the SAT trends in the ensemble simulations into four components: the forced thermodynamic response, the forced dynamic response, the internal thermodynamic response, and the internal dynamic

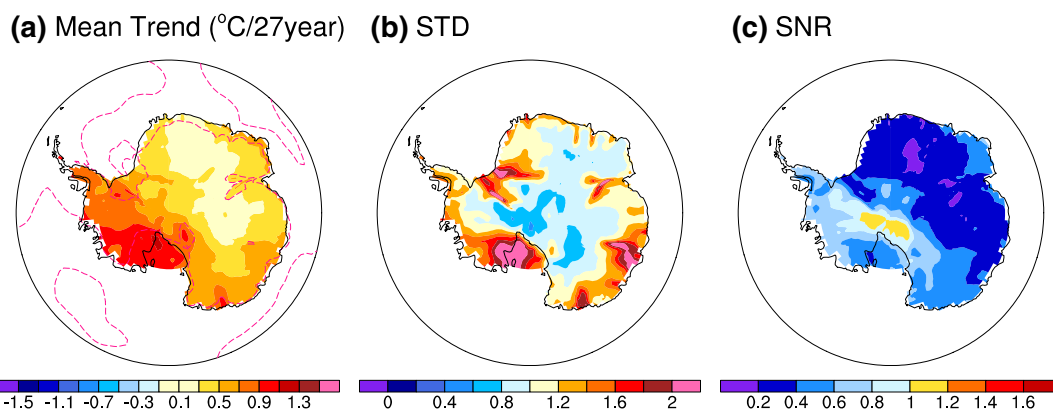


Fig. 3 **a** The ensemble-mean SAT trends ($^{\circ}\text{C}/27\text{ yr}$; 1979–2005) and SLP trends (contour interval 50pa) of the CESM simulations. Dashed lines represent negative SLP trends. **b** The standard deviation of the

SAT trends across 30 members. **c** The signal-to-noise ratio of the SAT trends in the CESM simulations

response. The procedure for the decomposition is listed as follows. First, the SAT trend related to large scale circulation change in each member is removed based on partial least-square regression (Wallace et al. 2012, see Method). According to Wallace et al. (2015), the residual SAT trend is related to the thermodynamic process while the removed part is linked to the dynamic process, thus being considered as the thermodynamically-induced trend and dynamical-induced trend, respectively. Second, we make an ensemble mean of all the 30 members of the thermodynamically-induced trend. The SAT trend related to internal thermodynamic variability will be averaged out and leave only a forced thermodynamically-induced SAT trend. Third, we make an ensemble mean of all the 30 members of the raw SAT trend, in which the internal variability will be averaged out and leave only a forced SAT trend. The difference between the forced SAT trend and the forced thermodynamically-induced trend is considered as the forced dynamically-induced trend. Fourth, the difference between the thermodynamically-induced trend in the first step and the forced thermodynamically-induced trends is the internal thermodynamic response, and the difference between the dynamical-induced trends and the forced dynamically-induced trend is the internal dynamic response.

Both the forced thermodynamically-induced (Fig. 4a) and the forced dynamically-induced SAT trends (Fig. 4b) are positive over all the regions in Antarctica, with the regional mean values of 0.20 $\text{k}/27\text{ yr}$ and 0.33 $\text{k}/27\text{ yr}$, respectively. The forced thermodynamically induced SAT trends are quite uniform over Antarctica. By contrast, the forced dynamically-induced SAT trends are larger in West than East Antarctica, especially in the west of Ross Ice Shelf, which is dynamically consistent with the ensemble-mean SLP trends. The forced dynamically-induced greater warming in West than in East Antarctica is similar to the observed trend in

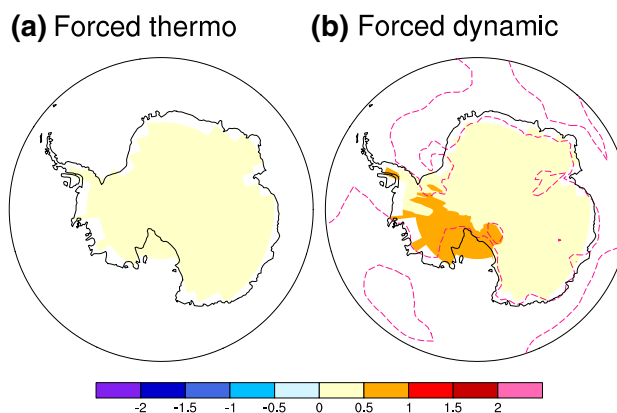
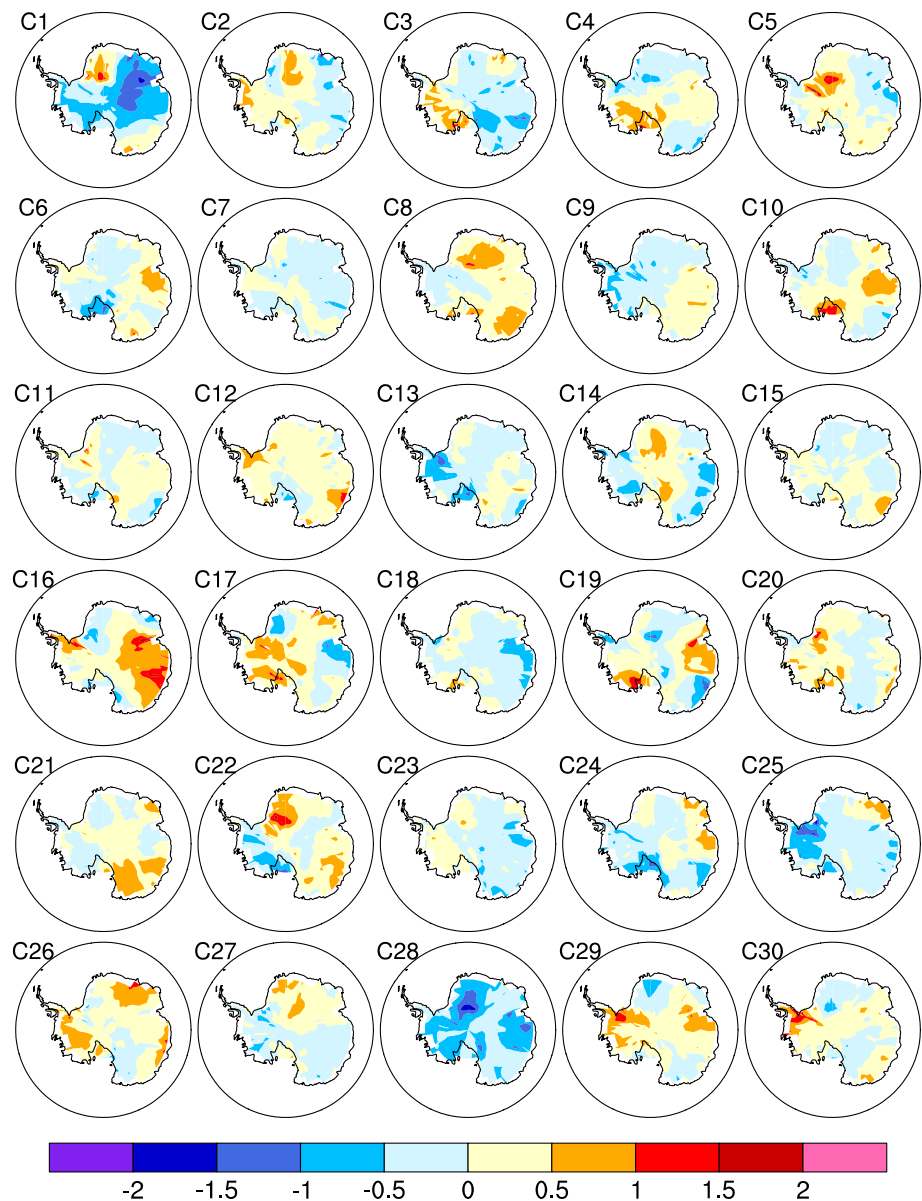


Fig. 4 **a** The forced thermodynamic response of SAT ($^{\circ}\text{C}/27\text{ yr}$; 1979–2005). **b** The forced dynamic response of SAT ($^{\circ}\text{C}/27\text{ yr}$; 1979–2005) and SLP (contour interval 50pa). Dashed lines represent negative SLP trends

spatial pattern but much weaker in amplitude, suggesting that the observed JJA Antarctic SAT trends are likely partly due to the external-forced atmospheric circulation changes. Figures 5 and 6 show the internal thermodynamically-induced and the internal dynamically-induced SAT trends in the 30 individual members, respectively. Both of them exhibit strong member-to-member and spatial diversity.

To quantify the relative influence of the four components on SAT trends in each grid, we take the sum of the absolute value of the forced thermodynamic response, the absolute value of the forced dynamic response, the standard deviation of the internal dynamic response across the members, and the standard deviation of the internal thermodynamic response, and calculate the percentage of each component. As shown in Fig. 7, the standard deviation of the internal response is larger than the absolute value of the forced response, indicating that internally generated SAT trends

Fig. 5 The internal thermodynamic response of SAT ($^{\circ}\text{C}/27$ yr; 1979–2005) among 30 members



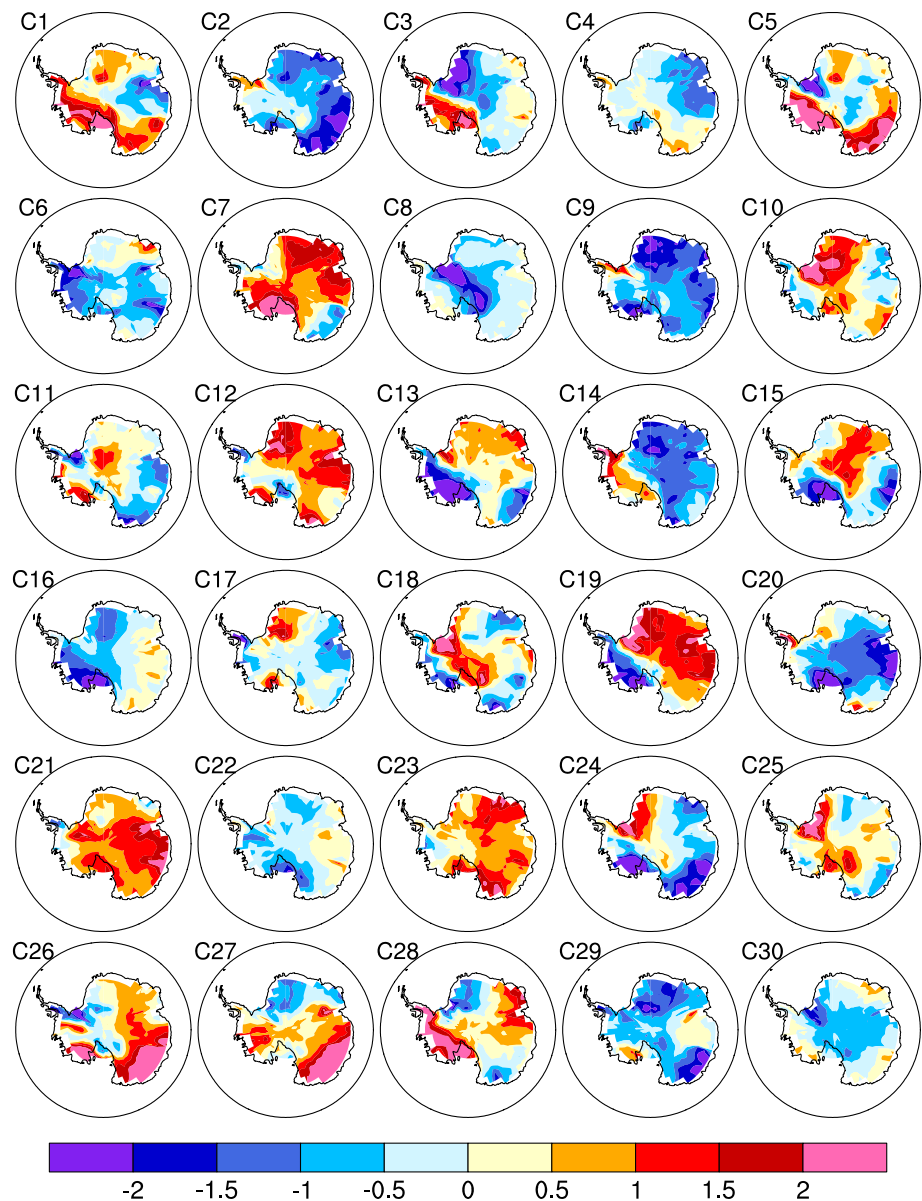
are larger than the forced SAT trends over Antarctica in the simulations. Moreover, the standard deviation of the internal dynamic response is almost two times larger than the standard deviation of the internal thermodynamic response, suggesting much of the internally generated variability in the SAT field is mediated by changes in the atmospheric circulation.

5 The external and internal variability of SAT trends in the Reanalysis data

We also apply the “dynamical adjustment” method (Method) to ERA-Interim (1979–2005) and Merra Reanalysis (1979–2005) following Wallace et al. (2012). The

ERA-Interim, as mentioned earlier, has a strong SAT trend (Fig. 8a). In the western part of the ice shelf, there is a warming trend greater than $2^{\circ}\text{C}/27$ yr, while the peninsula shows a cooling trend. The dipole mode in West Antarctica and the Peninsula is accompanied by a high-pressure system, locating around the Ross Sea. Figure 8b displays the thermodynamic part, which features warming trends in the west of the Ross Ice Shelf by $2^{\circ}\text{C}/27$ yr, but light cooling trends in much of East Antarctica. For the dynamic part (Fig. 8c), the SAT pattern is quite similar to that in the raw data, with strong warming in the west of the Ross Ice Shelf and cooling in the Peninsula. Near the ice shelf, we find that both thermodynamic and dynamic trends contribute more than $2^{\circ}\text{C}/27$ yr to its warming trend, while in the other regions, the dynamic part plays a

Fig. 6 The internal dynamic response of SAT ($^{\circ}\text{C}/27\text{ yr}$; 1979–2005) among 30 members



major role. For the Merra data, strong SAT warming trends distribute in and around the Ross ice shelf, cooling trends in the peninsula (Fig. 8d). After decomposition, the thermodynamic component is very small, between -0.5 and $0.5\text{ }^{\circ}\text{C}/27\text{ yr}$, and the raw trends are mainly determined by the dynamic component.

Although SAT trends in the two datasets are inconsistent with observations in some parts of Antarctica, both of them are mainly controlled by the change of atmospheric circulation. The forced thermodynamic components in the two reanalysis datasets are not consistent with each other, and both of them are different from the thermodynamically induced SAT trends in the ensemble simulations. This inconsistency would impair our understanding of what are the real thermodynamically induced SAT trends in recent decades.

6 The sources for the internal variability in the multidecadal SAT trend in the simulations

To identify the relationship between internal variability in JJA Antarctic SAT trends and the change of atmospheric circulation, we perform an SVD analysis on the SAT trends and Southern Hemisphere SLP trends during the period of 1979–2005 among the 30-member simulations. The first SVD mode accounts for 78.7% of the total explained variance, and the time series of the two fields are highly correlated, with the homogenous correlation coefficient about 0.83 (passing 99% confidence level). The first right heterogeneous mode features a SAM-like pattern in SLP trend (Fig. 9a), with high anomalies over Antarctica and almost

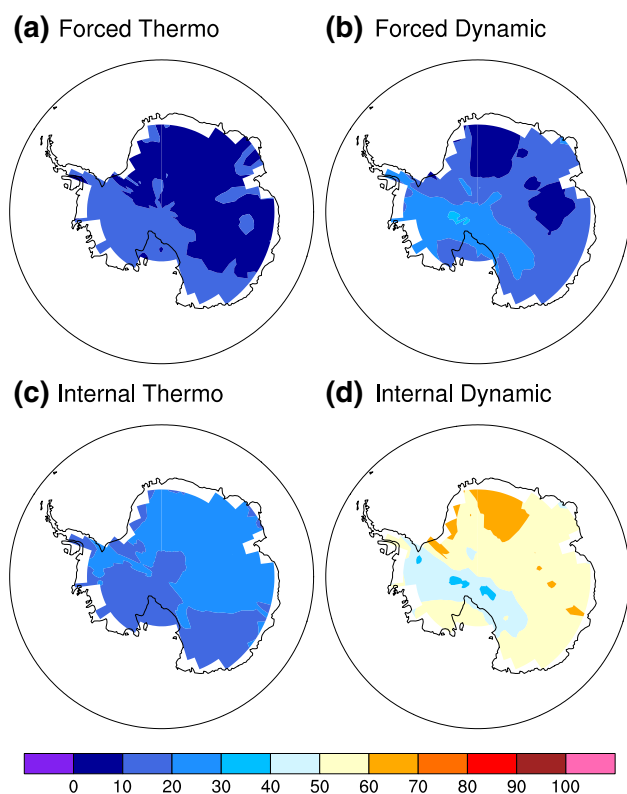


Fig. 7 The percentage of forced thermodynamic (a; %), forced dynamic (b; %), internal thermodynamic (c; %), internal dynamic (d; %) contribution in the total

annular low-pressure anomalies over the mid-latitudes. The highest SLP center locates in the sector of the South Pacific at around 60°S. The related SAT displays a coherent warming trend almost in all Antarctica except for a cooling trend in the Antarctic Peninsula (Fig. 9b). The SAT trend is dynamically consistent with the SLP trend. As shown in Fig. 9b, corresponding to the high-pressure center in the Southern Pacific, there is a southerly wind anomaly over the Antarctic Peninsula and northerly wind anomalies over the west of Ross ice shelf. The wind anomalies can lead to warm temperature advection over the west of Ross ice shelf and cold temperature advection over the Peninsula. Therefore, the SAT change in SVD1 is likely to be modulated by the SLP change around Antarctica.

Figure 10a shows the regression of 200 hPa geopotential height trends onto the time series of SLP trend filed in the SVD1. Consistent with the SLP trends, the 200 hPa geopotential height (Z200) trends also show an annular dipole structure between the high latitudes and the middle latitudes. Apart from the zonal symmetrical part, the regression pattern in Z200 trends features a notable wave structure in the sector of South Pacific, which corresponds to a wave fluxes propagating from New Zealand to the Ross Sea and to the Cape Horn. There are not significant wave fluxes

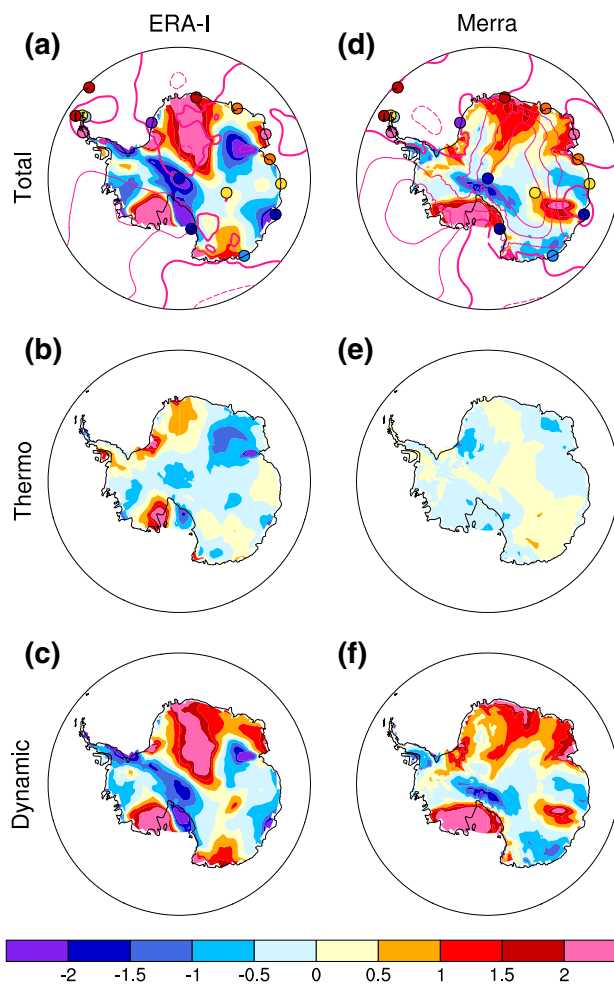


Fig. 8 Decomposition of the SAT trend ($^{\circ}\text{C} /27\text{y}$) of the reanalysis datasets. The left column is the ERA-Interim SAT trend (a–c; $^{\circ}\text{C} /27\text{yr}$), the right column is the Merra SAT trend (d–f). The first row is the total contribution (a, d), the second row is the thermodynamic response (b, e), the third row is the dynamic part (c, f). Contours in the first row represent SLP trends at interval of 200pa, solid lines represent positive SLP trends and dashed lines represent negative SLP trends

propagating from the Tropics, suggesting the SVD1 model is not affected much by tropical variability. Indeed, the correlations of SST trends with the time series of SLP trend filed in the SVD1 is weak in the Tropics (Fig. 10b). The significant SST correlations are mainly distributed in the midlatitudes over Southern Hemisphere, featuring a negative value belt in the sector of the Indian Ocean and the Pacific, while the correlations in the other oceans are rather weak. The negative SST trends in the midlatitude South Indian Ocean and the midlatitude South Pacific is likely caused by the weakening of SAM. As suggested by Alory et al. (2007), the weakening of SAM could lead to a northward shift of the subtropical gyre, which in turn leads to deep-reaching midlatitude cooling.

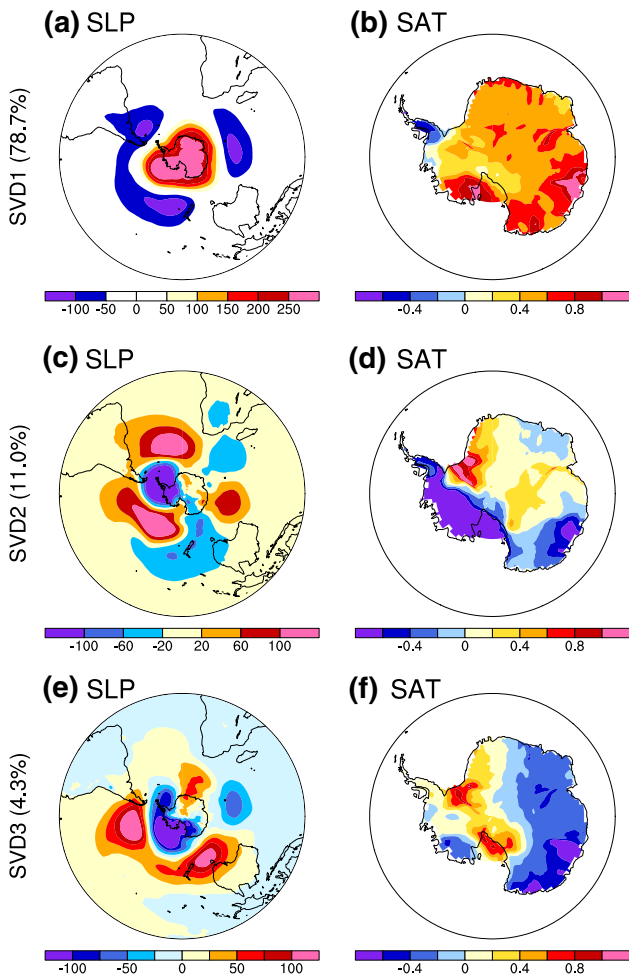


Fig. 9 The first leading SVD heterogeneous modes of SLP(a; hpa/27 yr) and SAT (b; °C /27 yr). The second mode of SLP (c; hpa/27 yr) and SAT (d; °C /27 yr). The third mode of SLP (e; hpa/27 yr) and SAT (f; °C /27 yr)

To confirm whether the SAM-like multidecadal change arises from atmospheric internal variability, we perform an EOF analysis on the SLP trends in a 2600-yr AGCM simulation, which is forced by a fixed annual cycle SST. The trends of SLP are calculated for 27-year periods obtained by dividing 2600 years into 96 consecutive sections, then EOF is performed upon these 96 samples. The first EOF mode (Fig. 11), accounting for 32.8% of the total explained variance, features a SAM like pattern. As the AGCM is forced by fixed annual cycle SST, the EOF modes of SLP trends must arise from atmospheric internal variability. The result indicates that the SAM-like pattern is the major atmospheric internal variability on the multidecadal time scale.

The second SVD mode in CESM ensemble simulations explains 11.0% of the total explained variance. Figures 9c and d show the pattern of SLP trends and SAT trends in the SVD2 mode. The SLP trend features a negative center to the east of Australia, a positive belt in the midlatitudes,

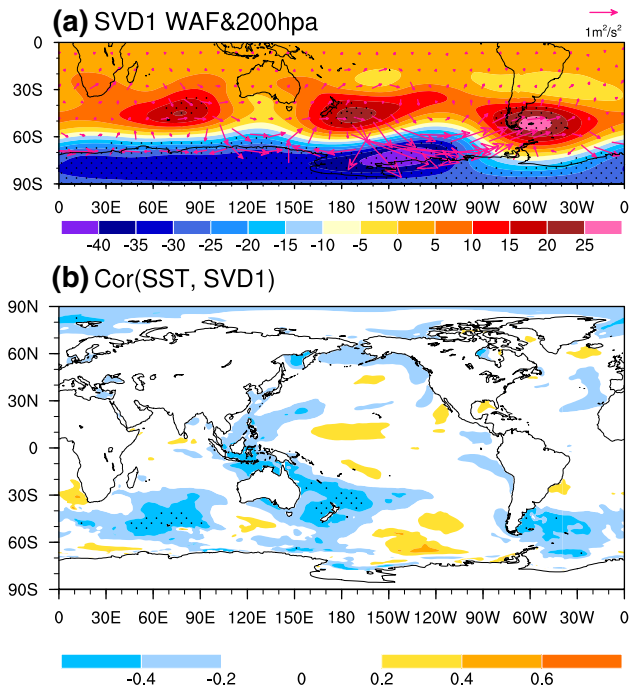


Fig. 10 a The regression of SLP (hpa/27 yr) on the time series of SLP in the first mode. b The regression of 200hp geopotential height (m/27 yr) onto the time series of SLP in the first mode and the associated wave active flux (vector; m^2/s^2). c The correlation between SST and the time series of SLP field in the first mode (color), the dots suggest passing the 95% confidence level

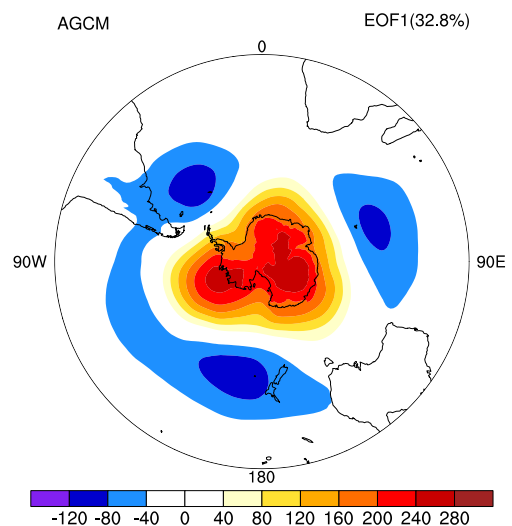


Fig. 11 Regression of SLP (Pa/27 yr) trends on the PC of AGCM of the first EOF mode

and a negative center in the Antarctic Peninsula. Associated with SLP trend anomalies, the ASL over the Antarctic Peninsula deepens, leading to anomalous northern winds over the Antarctic Peninsula and anomalous southern winds in

the east of the Antarctic Peninsula. Consequently, the SAT shows cooling trends in the Antarctic Peninsula and warm trends in the east of the peninsula. At 200 hPa, the SVD2 mainly corresponds to a 3-wave structure in geopotential height trends over the South Ocean (Fig. 12a). In the sector of Pacific, there are prominent southeastward wave fluxes from the tropical western Pacific to the Antarctic Peninsula, accompanied by significant warming trends in the tropical western and central Pacific (Fig. 12b). The result suggests that the SVD2 is likely to relate to the multidecadal variability in the tropical western and central Pacific. Compared to the observed Z200 trends associated with the central Pacific warming in recent decades (Ding et al. 2011), the SVD2-related Z200 trends show similar high anomalies over the tropical western Pacific and low anomalies over New Zealand, but the high anomalies over the high-latitude South Pacific shift northward about 10 latitudes relative to the observed trends. The difference in circulation trends, in turn, leads to different SAT trends over the western part of Antarctica compared to the observed trends.

The third SVD mode in CESM ensemble simulations only explains 4.3% of the total variance. Figure 9e and f show the pattern of SLP trends and SAT trends in the SVD3 mode. The SLP field mainly shows a dipole structure in the southern Pacific, with positive trends in the latitudes from 25°N

to 50°N and negative trends from 60°N to 80°N. The ASL in the SVD3 is also deepened, however, the latitudinal location is different from that in SVD2. In SVD3, ASL arrives at 120°W, which brings northern wind over the Antarctic Peninsula and leads to warming trends in this area. The SVD3 also corresponds to a 3-wave structure in Z200 trends (Fig. 13a), which is in quadrature with those in the SVD2. In the Tropics, the SVD3 is related to significant cooling trends in the tropical eastern Pacific (Fig. 13b). However, there are not southward wave fluxes from the tropical eastern Pacific to Antarctica, but on the contrary, there are northward fluxes into the tropical eastern Pacific. So, the causal relationship between SVD3 and climate variability in the tropical eastern Pacific is unclear.

The above results denote that the diversity of the simulated multidecadal Antarctic SAT trends among the 30-member simulations is mainly mediated by the SAM-like atmospheric circulation changes. Does the result depend on model selection? To answer this question, we also performed an SVD analysis between the SAT and the SLP trends (1979–2005) among 27 CMIP5 models (Fig. 14). The first SVD mode accounts for 77% of the total explained variance. The pattern of SLP trend features a dipole mode between Antarctica and the mid-latitudes, and the pattern of SAT trend shows negative anomalies in the Antarctic Peninsula

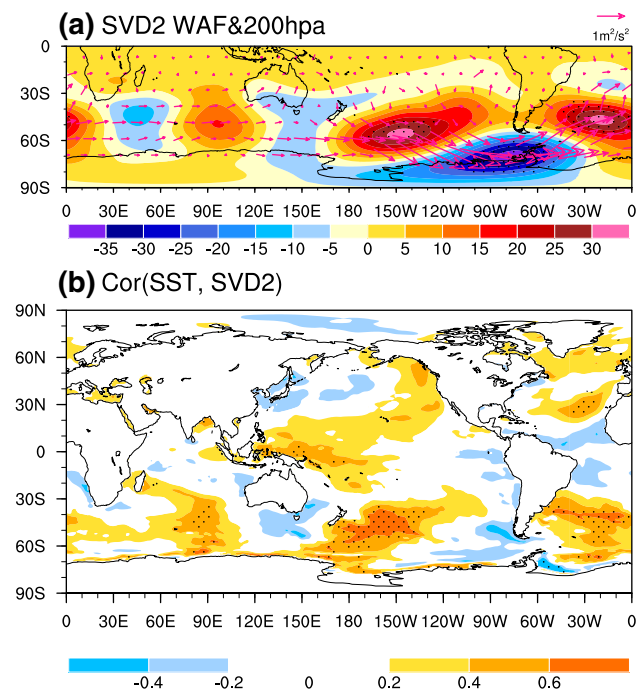


Fig. 12 a The regression of 200hp geopotential height (m/27 yr) onto the time series of SLP in the second mode and the associated wave active flux (vector; m²/s²). b The correlation between SST and the time series of SLP field in the second mode (color), the dots suggest passing the 95% confidence level

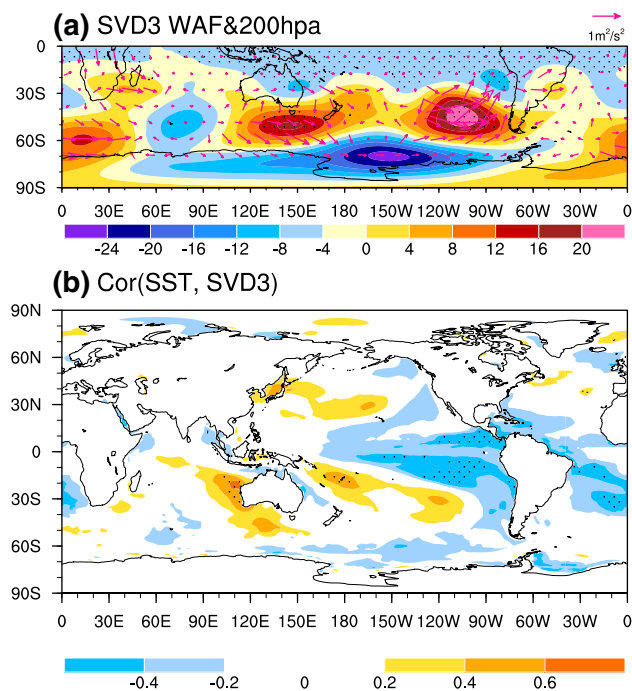


Fig. 13 a The regression of 200hp geopotential height (m/27 yr) onto the time series of SLP in the third mode and the associated wave active flux (vector; m²/s²). b The correlation between SST and the time series of SLP field in the third mode (color), the dots suggest passing the 95% confidence level

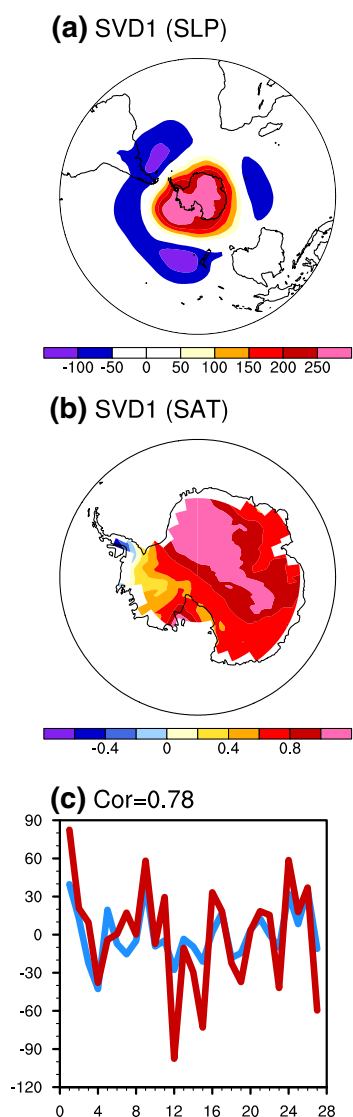


Fig. 14 The first leading SVD heterogeneous modes of SAT (color in **a**; °C /27 yr) and SLP (color in **b**; hpa/27 yr), and the time series (**c**) of the first leading modes in CMIP5 models

and positive anomalies in other regions, which are similar to the results produced by the CESM large ensemble. The result demonstrates that the relationship between SLP trends and the SAT trends does not depend on models very much.

7 Conclusion and discussion

In this study, we study the role of internal variability in the multidecadal changes of JJA Antarctic SAT using large ensemble simulations by CESM. The 30-member CESM simulations share the same external forcing and only differ in initial conditions. Hence, the ensemble-mean changes can represent the externally forced climate change, and the

diversity among individual members should be attributed to the internal variability. For the 1979–2005 JJA Antarctic SAT trends, there exists considerable diversity among individual ensemble members. In much of Antarctica, the standard deviation of the diversity is larger than the ensemble-mean trends, suggesting the multidecadal SAT trends are substantially affected by internal variability at this interval.

Moreover, we divide the SAT trends in the ensemble simulations into four parts: the forced thermodynamic response, the forced dynamic response, the internal thermodynamic response, and the internal dynamic response. In response to the externally forced factors, there are warming trends in all Antarctica in both the forced thermodynamic response and the forced dynamic response, with the regional mean values of 0.20 k /27 yr and 0.33 k/27 yr, respectively. Over West Antarctica, the forced dynamic response is much larger than the forced thermodynamic response, indicating the externally-forced warming in this area is mainly mediated by changes in atmospheric circulation. For the internal variability, the standard deviation of the internal dynamic response is almost two times larger than the standard deviation of the internal thermodynamic response, suggesting the internally generated variability at this interval mainly originates from internal variability in the atmospheric circulation in the simulations. In addition, the result from the two reanalysis datasets also demonstrates that the JJA Antarctic SAT trends during 1979–2005 are related to the change of atmospheric circulation.

Utilizing the SVD method, we identified the leading modes in the relationship between internal variability in JJA Antarctic SAT trends and the change of atmospheric circulation across the 30 individual members in CESM simulations during 1979–2005. The first leading mode in SLP trends features a SAM-like pattern. When there is a positive–negative seesaw of pressure trend between the polar and the mid-latitudes, the SAT trend is positive over most Antarctica but negative over the Antarctic Peninsula, and vice versa. Using an AGCM forced by a fixed annual cycle SST, we find that this SAM-like mode mainly arises from atmospheric internal variability rather than remote tropical SST. The second and third SVD modes in the CESM ensemble simulations only explain 11.0% and 4.3%, respectively. The SVD2 mainly corresponds to a 3-wave structure in geopotential height trends over the South Ocean. The wave train is likely to relate to the multidecadal variability in the tropical western and central Pacific. For the SVD3, there also exists a 3-wave structure in Z200 trends, which are in quadrature with those in the SVD2. Although SVD3 is related to significant cooling trends in the tropical eastern Pacific, there are not southward wave fluxes from the tropical eastern Pacific to Antarctica. So, the causal relationship between SVD3 and climate variability in the tropical eastern Pacific is still unclear and needs further research. The CESM simulations

can reproduce the observed teleconnection between the Tropics and Antarctica (Ding et al. 2011) to some extent, but the locations of anomalous center depart from the observations especially at high latitudes. The inconsistency deserves further study in the future.

Acknowledgements The authors would like to thank Xichen Li and Renguang Wu for many useful discussions. We also thank Letian Gu for reviewing a draft of this manuscript and Ruyu Gan for sharing the CESM1 dataset. The study is jointly supported by the National Key R&D Program of China (2018YFA0605904 and 2019YFA0606703), the Strategic Priority Research Program of Chinese Academy of Sciences (XDA20060502), the National Natural Science Foundation of China (41425086, 41831175, 41661144016, 41706026, 41506003, and 41731173), and Key Deployment Project of Centre for Ocean Mega-Research of Science, Chinese Academy of Sciences (COMS2019Q03).

Compliance with ethical standard

Conflict of interest The authors declare no conflict of interests.

References

- Alory G, Wijffels S, Meyers G (2007) Observed temperature trends in the Indian Ocean over 1960–1999 and associated mechanisms. *Geophys Res Lett* 34:471–473
- Arblaster JM, Meehl GA (2006) Contributions of external forcings to southern annular mode trends. *J Clim* 19:2896–2905. <https://doi.org/10.1175/Jcli3774.1>
- Berrisford P et al (2011) The ERA-Interim archive Version 2.0. ECMWF, Shinfield Park, Reading
- Deser C, Phillips A, Bourdette V, Teng HY (2012) Uncertainty in climate change projections: the role of internal variability. *Clim Dyn* 38:527–546. <https://doi.org/10.1007/s00382-010-0977-x>
- Deser C, Terray L, Phillips AS (2016) Forced and internal components of winter air temperature trends over North America during the Past 50 Years: mechanisms and implications. *J. Climate* 29:160107131720009
- Ding QH, Steig EJ, Battisti DS, Kuttel M (2011) Winter warming in West Antarctica caused by central tropical Pacific warming. *Nat Geosci* 4:398–403. <https://doi.org/10.1038/Ngeo1129>
- Fogt RL, Perlwitz J, Monaghan AJ, Bromwich DH, Jones JM, Marshall GJ (2009) Historical SAM variability Part II: twentieth-century variability and trends from reconstructions, observations, and the IPCC AR4. *Models J Climate* 22:5346–5275. <https://doi.org/10.1175/2009jcli2786.1>
- Hawkins E, Sutton R (2009) The potential to narrow uncertainty in regional climate predictions. *Bull Amer Meteorol Soc* 90:333–337
- Hawkins E, Sutton R (2011) The potential to narrow uncertainty in projections of regional precipitation change. *Clim Dyn* 37:407–418. <https://doi.org/10.1007/s00382-010-0810-6>
- Hu K, Huang G, Xie S-P (2018) Assessing the internal variability in multi-decadal trends of summer surface air temperature over East Asia with a large ensemble of GCM simulations. *Clim Dyn*. <https://doi.org/10.1007/s00382-018-4503-x>
- Ivy DJ, Hilgenbrink C, Kinnison D, Plumb RA, Sheshadri A, Solomon S, Thompson DWJ (2017) Observed changes in the Southern Hemispheric circulation in May. *J Clim* 30:527–527. <https://doi.org/10.1175/Jcli-D-16-0394.1>
- Kay JE et al (2015) The community earth system model (CESM) large ENSEMBLE project a community resource for studying climate change in the presence of internal climate variability. *Bull. Amer Meteorol Soc* 96:1333–1349. <https://doi.org/10.1175/bams-d-13-00255.1>
- Lehner F et al (2020) Partitioning climate projection uncertainty with multiple large ensembles and CMIP5/6. *Earth Syst Dynam* 11:491–508. <https://doi.org/10.5194/esd-11-491-2020>
- Li X, Holland DM, Gerber EP, Yoo C (2014) Impacts of the north and tropical Atlantic Ocean on the Antarctic Peninsula and sea ice. *Nature* 505:538. <https://doi.org/10.1038/nature12945>
- Li XC, Holland DM, Gerber EP, Yoo C (2015) Rossby waves mediate impacts of tropical oceans on west antarctic atmospheric circulation in Austral Winter. *J Clim* 28:8151–8164. <https://doi.org/10.1175/Jcli-D-15-0113.1>
- Marsh DR, Mills MJ, Kinnison DE, Lamarque J-F, Calvo N, Polvani LM (2013) Climate Change from 1850 to 2005 Simulated in CESM1(WACCM). *J Climate* 26:7372–7391. <https://doi.org/10.1175/jcli-d-12-00558.1>
- Raphael MN et al (2016) The amundsen sea low variability Change, and Impact on Antarctic Climate. *Bull Amer Meteorol Soc* 97:111–121. <https://doi.org/10.1175/bams-d-14-00018.1>
- Rienecker MM et al (2011) MERRA: NASA's modern-era retrospective analysis for research and applications. *J Climate* 24:2724–2748. <https://doi.org/10.1175/jcli-d-11-00015.1>
- Schneider DP, Deser C (2018) Tropically driven and externally forced patterns of Antarctic sea ice change: reconciling observed and modeled trends. *Clim Dyn* 50:4599–4618. <https://doi.org/10.1007/s00382-017-3893-5>
- Schneider DP, Deser C, Okumura Y (2012) An assessment and interpretation of the observed warming of West Antarctica in the austral spring. *Clim Dyn* 38:323–347. <https://doi.org/10.1007/s00382-010-0985-x>
- Seviour WJM, Gnanadesikan A, Waugh DW (2016) The transient response of the southern ocean to stratospheric ozone depletion. *J Clim* 29:7383–7396. <https://doi.org/10.1175/Jcli-D-16-0198.1>
- Takaya K, Nakamura H (2001) A formulation of a phase-independent wave-activity flux for stationary and migratory quasigeostrophic eddies on a zonally varying basic flow. *J Atmos Sci* 58(6):608–627
- Taylor KE, Stouffer RJ, Meehl GA (2012) An overview of Cmp5 and the experiment design. *Bull Amer Meteorol Soc* 93:485–498. <https://doi.org/10.1175/Bams-D-11-00094.1>
- Thompson DWJ, Solomon S, Kushner PJ, England MH, Grise KM, Karoly DJ (2011) Signatures of the Antarctic ozone hole in Southern Hemisphere surface climate change. *Nat Geosci* 4:741. <https://doi.org/10.1038/ngeo1296>
- Turner J et al (2004) The SCAR READER project: toward a high-quality database of mean antarctic meteorological observations. *J Clim* 17:2890–2898. [https://doi.org/10.1175/1520-0442\(2004\)017%3C2890:tsrpta%3E2.0.co;2](https://doi.org/10.1175/1520-0442(2004)017%3C2890:tsrpta%3E2.0.co;2)
- Wallace JM, Deser C, Smoliak BV, Phillips AS (2015) Attribution of climate change in the presence of internal variability. In: climate change: multidecadal and beyond. World Scientific, pp 1–29 https://doi.org/10.1142/9789814579933_0001
- Wallace JM, Fu Q, Smoliak BV, Lin P, Johanson CM (2012) Simulated versus observed patterns of warming over the extratropical Northern Hemisphere continents during the cold season. *P Natl Acad Sci USA* 109:14337–14342. <https://doi.org/10.1073/pnas.1204875109>

Publisher's Note Springer Nature remains neutral with regard to jurisdictional claims in published maps and institutional affiliations.